



ELSEVIER

Available online at [www.sciencedirect.com](http://www.sciencedirect.com)

SCIENCE @ DIRECT®

Combustion and Flame 142 (2005) 276–288

Combustion  
and Flame

[www.elsevier.com/locate/combustflame](http://www.elsevier.com/locate/combustflame)

# The influence of a cerium additive on ultrafine diesel particle emissions and kinetics of oxidation

Heejung Jung, David B. Kittelson, Michael R. Zachariah\*

*Departments of Mechanical Engineering and Chemistry, University of Minnesota, 111 Church Street SE, Minneapolis, MN 55455, USA*

Received 9 March 2004; received in revised form 2 November 2004; accepted 2 November 2004

Available online 30 April 2005

## Abstract

The influence of a cerium additive on the kinetics of oxidation and size distribution of ultrafine diesel particles was studied using a high-temperature oxidation-tandem differential mobility analysis method over the temperature range 300–700 °C. The addition of cerium to the diesel fuel was observed to cause significant changes in number-weighted size distributions, light-off temperature, and kinetics of oxidation. The peak number concentration in the accumulation mode decreased 50 and 65%, respectively, for 25 and 100 ppm dosing levels under 1400 rpm and 75% engine load. The light-off temperature was reduced by 250 and 300 °C, respectively, for 25 and 100 ppm dosing levels. The oxidation rate increased significantly ( $\times 20$ ) with the addition of cerium to the fuel; however, the rate was relatively insensitive to dosing level. The activation energy for cerium-dosed oxidation was, within experimental error, equivalent to that for undosed fuel ( $E_a = 100\text{--}110 \text{ kJ mol}^{-1}$ ). From a phenomenological kinetic rate perspective, the increase in oxidation rate was attributed solely to an increase in the preexponential factor. These results suggested that diesel particles using regular, undosed diesel fuels were already metal-catalyzed to some extent, most likely from metals in the lube oil. The addition of cerium likely increased the number of catalytic sites but had no effect on the overall activation energy due to the presence of other metals in the diesel particulate matter coming from lube oil. The characteristics of cerium-laden diesel particles were also investigated. Two principal types of aggregates were found using transmission electron microscopy and energy-dispersive spectrometry analysis. The first was composed mainly of agglomerates of carbonaceous spherules and a few, considerably smaller cerium oxide nanoparticles. The second consisted of metallic aggregates composed mainly of cerium oxide nanoparticles and some carbon.

© 2005 Published by Elsevier Inc. on behalf of The Combustion Institute.

*Keywords:* Cerium; Diesel; Additive; Oxidation; Kinetics; Emissions

## 1. Introduction

The increasing use of diesel combustion for powering passenger cars has led to considerable activ-

ity in methods for the reduction of particulate emissions. About one-third of the new passenger car market in Western Europe is diesel-powered. Even in the gasoline-dominant United States, modern diesel vehicles with new emission reduction systems are receiving increased interest. Part of this renewed interest is centered on a reduction of emissions from modern diesels and new abatement strategies and technolo-

\* Corresponding author.

E-mail address: [mrz@umd.edu](mailto:mrz@umd.edu) (M.R. Zachariah).

gies, e.g., diesel particulate filter, fuel additives for particulate matter reduction, and  $\text{NO}_x$  adsorber catalysts for  $\text{NO}_x$  reduction.

Diesel fuel additives, used to lower PM emissions and to enhance oxidation rates, are an approach that shows promise in improving emission reductions. In this article, we report on studies of a cerium-based fuel additive and the resulting particle size distribution. We also report on the use of a tandem differential mobility analyzer to determine size-selected oxidation rate and the role of cerium oxide on the rate of soot oxidation.

## 2. Background of soot abatement, oxidation, and the use of additives

Diesel particulate filters (DPFs) have been studied since the 1980s as a means to reduce or to eliminate diesel particulate matter (PM) emissions [1–3]. The DPF, however, requires periodical regeneration of the filtering material by oxidation of the filter deposit to prevent plugging. As the ignition temperature of the diesel PM bed is considerably higher than the exhaust gas temperatures of the diesel engine, the use of catalytic combustion to lower the ignition temperature has attracted interest. Most research has focused on either employing a filter coated with a catalyst or adding a catalyst additive directly to the fuel. The former method is limited by the problem of catalyst poisoning from the exhaust gas [4] and poor contact between the PM and catalytic surface. The additive approach is being studied in combination with DPFs or bulk soot samples. In these works, a variety of metal additives have been tested. Miyamoto et al. [5,6] investigated the effect of Ca, Ba, Fe, and Ni naphthenates. They found that Ca and Ba most efficiently reduced the soot, by both suppressing soot formation and enhancing soot oxidation. Valentine et al. [7] studied the catalytic effect of bimetallic Pt/Ce additives in an attempt to lower the dosing level of the metal additive down to 4 ppm to reduce ash loading on the DPF and the emission of metallic ultrafine particles. Skillas et al. [8] studied the effect of Ce and Fe on the size distribution and composition of diesel PM; they observed a reduction in the accumulation mode, but an increase in ultrafines. Lahaye et al. [9] studied the catalytic effect of Ce on simulated diesel PM oxidation and observed that the cerium was both on and within the soot as cerium oxides. Kasper et al. [10] added ferrocene to the fuel and speculated that the enhancement of oxidation was more effective in reducing soot than a suppression effect.

Many studies [11,12] have focused on the change in ignition temperature of the diesel PM bed with different metal additives. While these results are of

obvious practical benefit, it has been difficult to decouple the role of the catalyst on the increase in the oxidation rate from other effects that may also promote an increase in oxidation rate and a decrease in ignition temperature (e.g., the heat and mass transfer effect, particle size).

In view of the complex interrelationships discussed above, we have attempted to extract intrinsic oxidation kinetics in this article, to assess the role of the catalyst in reducing the ignition temperature and enhancement of the oxidation rate.

## 3. Experimental

### 3.1. Cerium additive, fuel, and lubrication oil

The cerium additive used was a nanoparticulate cerium oxide dispersed in an organic solvent to make it directly miscible with diesel fuel (product name Eolys DPX-9), and was provided by Rhodia Electronics & Catalysis. The manufacturer recommended using a dosing level of 25 ppm (of cerium in the fuel) by weight in combination with a DPF for a real-world application. For our studies, we also used a higher dosing level of 100 ppm to assess the effect of catalyst loading on the oxidation of diesel particles. For these studies, a standard EPA No. 2 on-road diesel fuel (300–500 ppm sulfur) was used as a base fuel. The lubricating oil used in this study was SAE15W-40 (John Deere TY6391).

### 3.2. Engine, sampling, and dilution system

The engine used in this study was a medium-duty, direct injection, four-cylinder, four-cycle, mid-1990s turbocharged diesel engine (John Deere T04045TF-250). It had 4.5-L displacement, with a peak power output of 125 HP (93 kW) at 2400 rpm and a peak torque output of 400 Nm at 1400 rpm. The output of the engine was coupled to a dynamometer for load control; the engine was operated at 1400 rpm under 75% load (300 Nm). The exhaust temperature measured at the exhaust manifold was  $\sim 560^\circ\text{C}$  and the measured air–fuel ratio was 27 for regular fuel at 1400 rpm under 75% load (300 Nm).

Fig. 1 is a schematic diagram of the engine bench, sampling system, scanning mobility particle sizer (SMPS) [13], and high-temperature oxidation–tandem differential mobility analyzer (HTO-TDMA) system [14]. The exhaust was sampled 25 cm downstream of the turbocharger exit and was diluted in a two-stage, air ejector, variable residence time dilution tunnel, similar to that described by Abdul-Khalek et al. [15]. For the oxidation study, particles were extracted after the first stage of dilution, which was

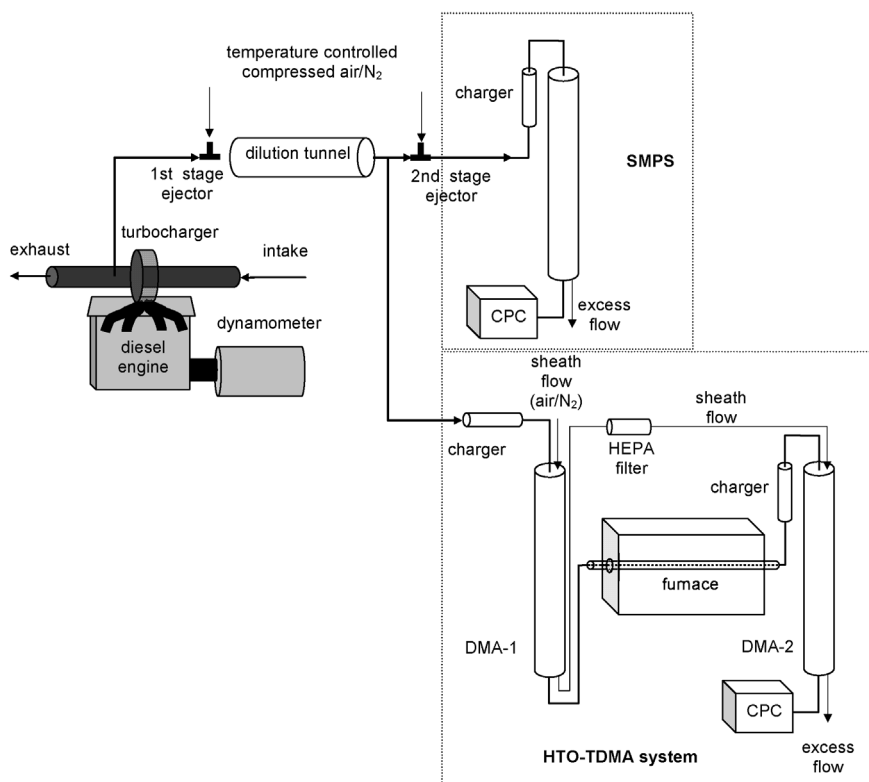


Fig. 1. Schematic diagram of the experimental setup. The bold line indicates the path taken by the diesel particles.

operated with a fixed residence time of 0.8 s at a dilution ratio of 26:1 to 28:1 for 75% load at 1400 rpm.

The first-stage dilution ratio was determined by comparing the  $\text{NO}_x$  concentration in the exhaust gas and that in the diluted exhaust gas; corrections were made for the background  $\text{NO}_x$  concentration. The first-stage dilution air temperature was maintained at 32 °C by preheating and temperature stabilizing the compressed air to the ejector.

For all size distribution studies, samples were taken after the second stage of dilution to prevent saturation of the condensation particle counter (CPC) (Model 3025A, TSI Inc.). The second-stage dilution ratio was determined by flow measurements to be 31:1. Thus, the overall dilution ratio after the second stage was 810:1 to 870:1, calculated by the product of dilution ratios from each stage.

### 3.3. Oxidation experiments and size distribution measurement

The sampled aerosol stream from the first stage of the dilution tunnel was either introduced into the HTO-TDMA for the oxidation study and/or subjected to second-stage dilution, prior to sampling by the SMPS as illustrated in Fig. 1. The HTO-TDMA was

described in detail in our previous study by Higgins et al. [14].

Briefly, in the HTO-TDMA, the sample is sent through a bipolar diffusion charger to establish a known charge distribution, then, a specific particle size is selected with DMA-1. The DMA selects mono-area particles based on electrical mobility. Previous studies [16,17], employing DMA size selection with TEM analysis, showed that the DMA selects for mono-area aggregates, and that the surface area determined by a DMA was equivalent to their projected area, for particles with mobility diameters under about 200 nm. These mono-area particles are oxidized in air by passing through a heated quartz tube for specified residence time and known time-temperature profile. The particles are recharged in a bipolar diffusion charger and the size change resulting from the high-temperature processing (which includes oxidation, thermal restructuring, and evaporation processes) is measured with scanning DMA-2. Three initial particle sizes of 41, 92, and 132 nm mobility diameters were selected at DMA-1 to match the previous study on diesel nanoparticle oxidation [14]. Furnace temperature settings ranged from room temperature (25–34 °C, depending on the day) to 700 °C.

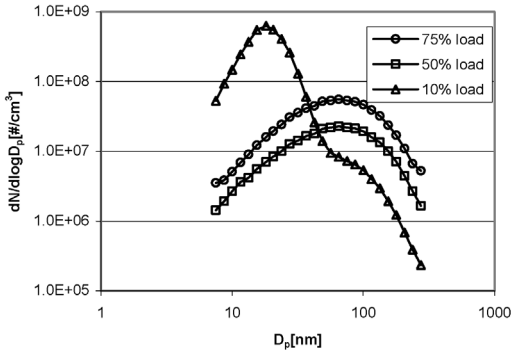


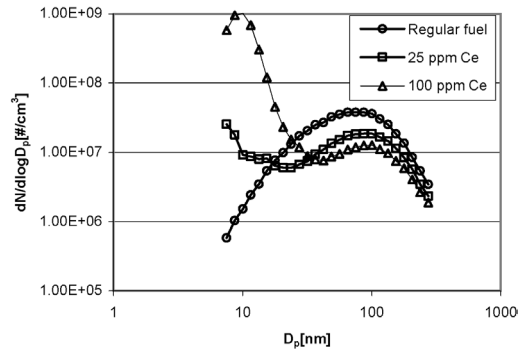
Fig. 2. Size distributions of diesel particles with base fuel for various engine loads at 1400 rpm.

To check for particle size changes due to thermal effects, additional experiments were conducted by using nitrogen as a carrier gas in both the first-stage dilution and DMA sheath flows in our previous study [14].

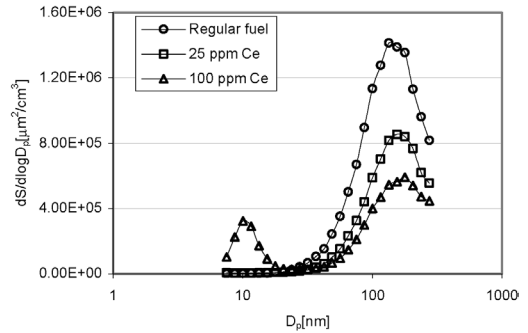
## 4. Results and discussion

### 4.1. Influence of cerium additive on the size distribution

Fig. 2 shows the size distributions (corrected for dilution ratio) of diesel soot as a function of engine load at 1400 rpm using regular diesel fuel. For the diesel engine used in these tests, particles at high engine load (75%) are mainly agglomerates (accumulation mode) over the whole size range, whereas particles at light engine load (10%) are composed of both nuclei and accumulation mode particles. These nuclei mode particles are primarily composed of volatile organics (for sizes below  $\sim 30$  nm), while the accumulation mode particles are agglomerates composed primarily of solid carbonaceous materials [18]. As the accumulation mode increased with increasing engine load, more particle surface area became available for vapor phase compounds to condense. As a result of the greater available surface area and higher exhaust temperature, higher engine loads resulted in a lower saturation ratio during the gas phase at the exhaust, and a lower rate of homogeneous nucleation or new particle formation. The latter point has been investigated in a study in which particles at light engine loads were sent to a catalytic stripper [19]. The catalytic stripper is a small catalytic converter that is maintained at constant temperature to enhance both the evaporation and the oxidation of volatile organics [19]. Volatile organics diffuse to and oxidize on the catalyst-coated wall of the stripper. Ng [20]



(a)



(b)

Fig. 3. Size distributions of diesel particles with cerium-dosed fuel for various dosing levels at 1400 rpm, 75% load. (a) Number distributions. (b) Geometric surface area distributions.

showed that nuclei mode particles could be significantly reduced by employing the catalytic stripper, indicating that the nuclei mode was overwhelmingly composed of volatile materials.

Fig. 3 shows the effect of the cerium additive on the particle size distribution for various dosing levels under fixed engine conditions (75% engine load (300 Nm) at 1400 rpm). The cerium additive clearly had a significant effect on reducing the number concentration of particles in the accumulation mode. A 50% reduction in peak concentration was observed at the 25 ppm dosing level, and a 65% reduction at the 100 ppm level. The relative insensitivity of the results to dosing level was qualitatively consistent with the work of Skillas et al. [8], who observed a significant reduction of particles in the accumulation mode at 20 ppm cerium, but saw no effect with further increases in cerium. While the accumulation mode clearly decreased, a dramatic increase in the nuclei mode was observed with the addition of cerium, which has also been confirmed by Skillas et al. [8]. This behavior is consistent with particle physics. A decrease in the accumulation mode, and therefore available surface area, as

shown in Fig. 3b, reduces scavenging of particle precursors, thus promoting homogeneous nucleation, while at the same time decreasing coagulation of nuclei mode particles with accumulation mode particles.

To understand this increase in the nuclei mode, we sent the undosed and 100 ppm-dosed particles to a catalytic stripper, operating at 300 °C. Fig. 4 shows that the nuclei mode particles were reduced, but did not disappear altogether; this suggests that the nuclei mode was composed of more than volatile organics. This is consistent with the observation of Skillas et al. [8], who, using inductively coupled plasma mass spectrometry (ICP-MS) found that nuclei mode particles are composed mostly of cerium.

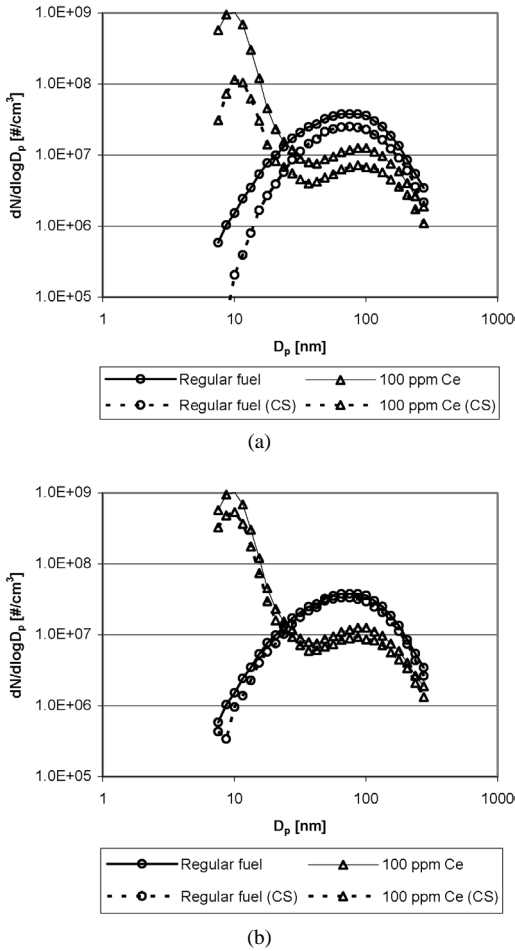


Fig. 4. (a) Size distributions of diesel particles before and after the catalytic stripper at 1400 rpm, 75% load without transport (diffusion and thermophoresis) loss correction. (b) Size distributions of diesel particles before and after the catalytic stripper at 1400 rpm, 75% load with transport loss correction. CS, catalytic stripper.

4.2. HTO-TDMA results

Fig. 5a shows representative HTO-TDMA data for 90-nm particles generated under 25 ppm cerium added fuel, under fixed engine conditions (75% engine load (300 N m), 1400 rpm). Results for other initial particle sizes at 25 and 100 ppm cerium are similar to those in Fig. 5a, but are not presented here; however, the results were used to deduce the oxidation rate presented later in the article. Fig. 5a illustrates that the particles shrink as furnace temperature increases; the mobility diameter decreased by 1 nm at 300 °C and by 7 nm at 650 °C. The total particle size decrease, due to nonoxidative effects at 500 °C, measured using nitrogen as the carrier gas, amounted to ~1 nm at 75% load using regular diesel [14]; this is consistent with the shrinkage we observed at 300 °C for cerium loading. The initial shrinkage below 300 °C is inconsistent with the kinetic results observed at higher temperatures and is likely due to the evaporation of semivolatile materials condensed on the diesel particles. Sakurai et al. [21] have also reported such shrinkage. Above 300 °C, most of the diameter change results from particle oxidation. In addition to a decrease in particle size with increas-

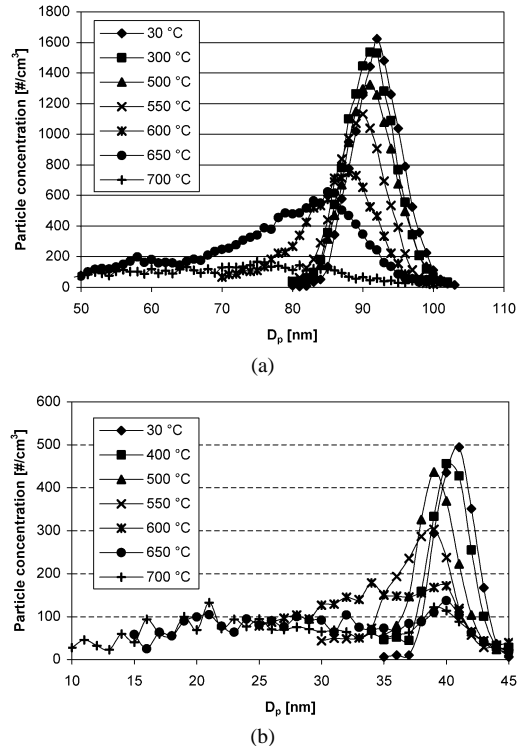


Fig. 5. TDMA diesel particle oxidation results in air for furnace settings of 30–700 °C: (a) 92-nm initial particle size with 25 ppm cerium-dosed fuel. (b) 41-nm initial particle size with 100 ppm cerium-dosed fuel.

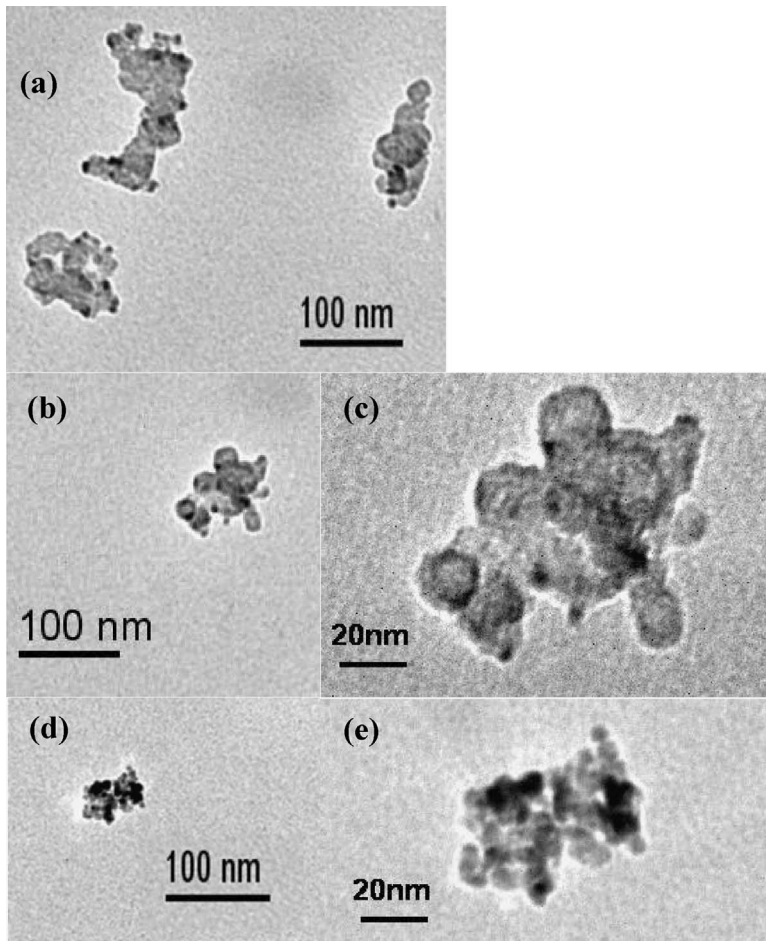


Fig. 6. TEM images of 50-nm mobility diameter, cerium-laden diesel particles. Particles were sampled under 75% load at 1400 rpm using a 100 ppm cerium doping level. (c) and (e) were taken at higher magnification.

ing oven temperature, we also observed a decrease or loss of particles. This decrease in number concentration was not associated with chemical reactivity, but, rather, thermophoretic transport losses, which become most important at higher temperatures [22]. In Fig. 5b, we see results for 40-nm particles at 100 ppm cerium. At higher oven temperatures, two modes were observed. In this case, rather than a steady decrease to smaller sizes by the primary peak, as observed in all our previous studies, here we saw a mode (e.g., at 600 and 650 °C) near 40 nm, and another peak at about 34 and 32 nm, respectively. This behavior may be attributed to the fact that some particles were composed primarily of cerium compounds that homogeneously condensed from the vapor and have an associated carbon coating. The mixture of 40-nm particles, predominately either cerium or carbon, resulted in a bimodal size distribution after oxidation. This is consistent with our TEM observation discussed later in the article.

Figs. 6 and 7 are TEM images of cerium-laden diesel particles under 75% engine load, 1400 rpm, at 100 ppm cerium. The procedure detailed in our previous study was used to sample particles on SiO<sub>2</sub>-coated nickel TEM grids [16]. In brief, the aerosol flow after the first stage of the dilution tunnel is sent to a DMA and the resulting monodisperse output is sent to a low-pressure impactor (LPI) [23]. Particles are collected on the TEM grid at the bottom stage of the LPI.

In Fig. 6 are shown 50-nm mobility diameter particles. Please note that Figs. 6a, 6b, and 6d were taken at the same magnification, whereas Figs. 6c and 6e are higher magnifications of Figs. 6b and 6d, respectively. The dark regions within the aggregates have been identified as predominantly cerium oxide. In general, we observed two classes of particles. The vast majority, i.e., those greater than ~80%, look morphologically like those shown in Figs. 6a–6c. These particles were characterized by carbonaceous aggregates deco-

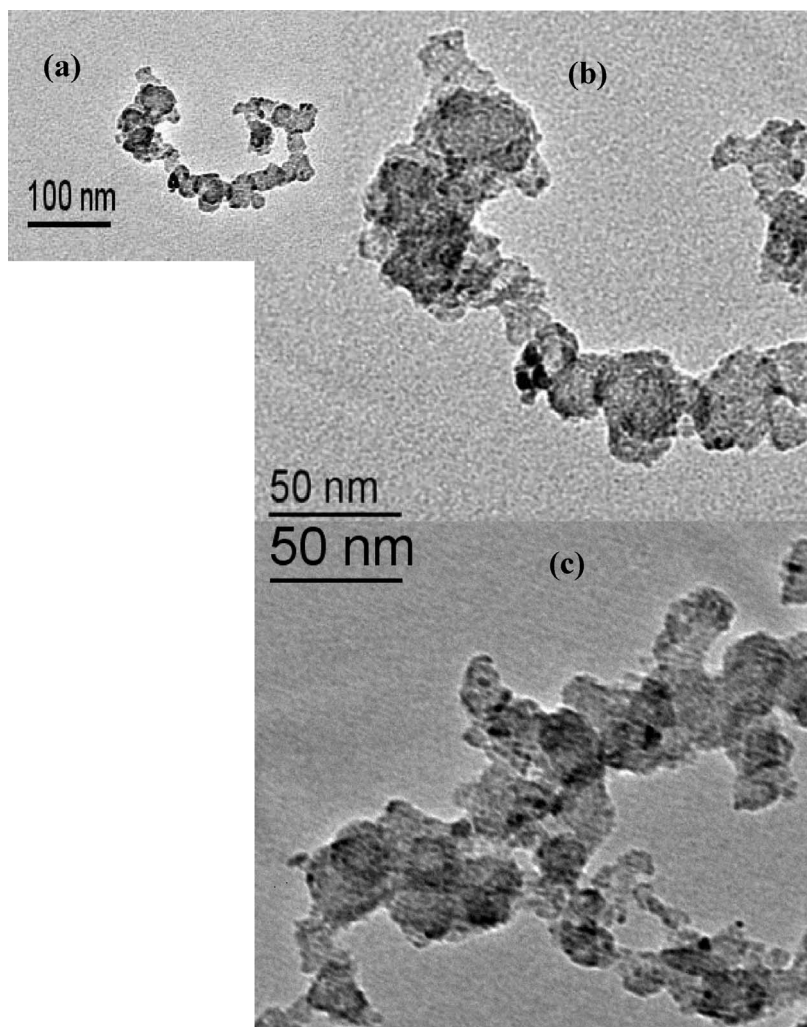


Fig. 7. TEM images of 130-nm mobility diameter, cerium-laden diesel particles. Particles were sampled under 75% load at 1400 rpm using a 100 ppm cerium doping level. (b) and (c) were taken at higher magnification.

rated on the surface with fine cerium oxide nanoparticles, nominally less than 5 to 7 nm in diameter. The other, much less prevalent class of particles is represented by Figs. 6d and 6e. These particles were characterized as having a larger fraction of cerium in the aggregate. In addition, these particles seemed to have much smaller primary particles (5–7 nm), as compared with the more prevalent class (~20 nm), while having a significantly larger fraction of cerium. Particles composed mainly of metallic compounds have also been observed in the nuclei mode when either lube oil (which contains metals) or ferrocene has been added to the diesel fuel [24].

We also observed these two classes of particles in our HTO-TDMA studies. Referring to Fig. 5b, we observed a bimodal distribution after oxidation at 700 °C. The first mode consisted of preselected

40-nm particles that remained after oxidation, while the other mode reflected shrinkage to ~20 nm. This is consistent with some particles exiting the engine being composed primarily of metal, as seen in Fig. 6d.

TEM images of 130-nm mobility diameter particles are shown in Figs. 7a–7c. These particles were far less compact than 50-nm mobility diameter particles. While the contrast is not as great in these images, compared with those in Fig. 6, very fine cerium particles, also in the range of 5 to 7 nm, can be seen on close inspection. The other class (metal aggregates) of particles was not observed at this larger mobility.

In Fig. 8 are two kinds of aggregates used for energy-dispersive spectroscopy (EDS) analysis. The one on the left is the carbonaceous aggregate, and the other on the right is the metal aggregate. The electron beam diameter is approximately the same as

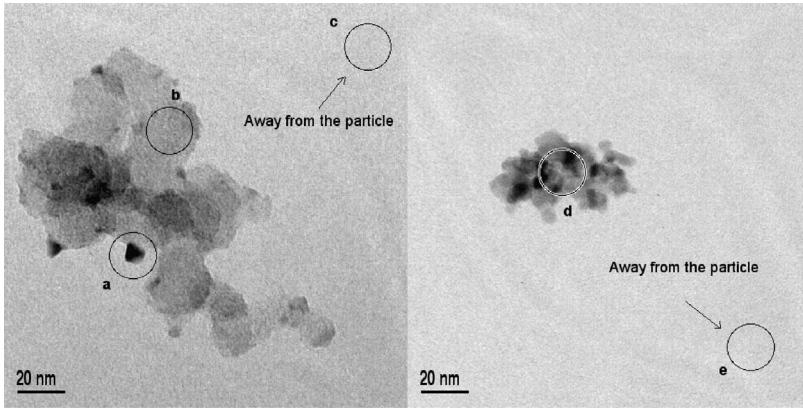


Fig. 8. TEM images of cerium-laden diesel particles for EDS. Background noise from the substrate was measured away from the particles (spots c and e) for correction of the spectrum.

the circles shown in Fig. 8. Background signals from a substrate were measured away from the particles. Fig. 9 shows the EDS spectrum for each spot marked in Fig. 8. In all EDS spectra, without correction for background signal, there are peaks for carbon (C), oxygen (O), silicon (Si), and nickel (Ni). This is expected, as  $\text{SiO}_2$ -coated nickel TEM grids were used. Spots a and d indicate very distinguishable Ce peaks, whereas other spots do not. Unfortunately, the Ce M peak (the third peak from the left in the spectrum for spot d) occurs at the same energy level (within the resolution of our EDS system) as the Ni L peak. Therefore, the Ni L peak is what is most visible, except for spots a and d, where the large Ce L peaks (three consecutive peaks in the middle of spectrum) indicate that there should be appreciable Ce M lines visible. Spot d, for the metal aggregate, exhibits high counts on Ce peaks; this indicates that it is composed mainly of Ce. The background signal was removed for the spectra of spots a, b, and d. Spot a, which was a soot particle associated with Ce nanoparticle, shows distinguishable peaks for carbon, cerium, and low counts for oxygen. Spot b, which was a mainly carbonaceous soot particle, exhibits a higher carbon peak than spot a and a low oxygen peak. Spot d, which was identified as a metallic aggregate, shows high peaks for cerium, oxygen, and carbon. These spectra suggest that the Ce in the particles was in the form of cerium oxide rather than pure cerium and that some carbon was also present. This is consistent with the prior study by Skillas et al. [8], who found Ce present as  $\text{CeO}_2$  in the ash of diesel PM (DPM) and proposed that cerium, like iron, reaches its highest oxidation state ( $\text{Ce}^{4+}$ ) very early, during the particle formation phase.

These metallic aggregates were also examined by electron diffraction. The diffraction pattern for the particle shown in Fig. 10a is shown in Fig. 10b. The well-defined pattern suggests that these metal aggre-

gates were composed of crystallites, rather than soot particles, which are normally identified as amorphous and result in no pattern. Fig. 10c is a dark-field image. The bright area is where the electron beam diffracted to show a pattern. Because orientations of crystallites are not homogeneous, the pattern is not regular.

The prominent feature of DPM from cerium-dosed fuels is that fine cerium oxide nanoparticles decorate the exterior of soot agglomerates. A nanoparticulate cerium oxide mixed with fuel should remain unchanged during diesel combustion due to its very high melting point (2200–2400 °C) (in other words, very low vapor pressure). There may be some agglomeration of particles as well as a partial reduction of Ce(IV). As dosing level increases, the concentration of accumulation mode particles decreases. This results in more cerium oxide nanoparticles surviving the scavenging by carbonaceous particles. Finally, because the total mass of particulate matter decreases on the addition of cerium, as evidenced in Fig. 4, enhanced oxidation, which of course proceeds from the exterior of the particles, results in aggregates of soot with the cerium decorating the surface, similar to what was observed in the TEM.

#### 4.3. Determination of the oxidation rate

Using the measured decrease in particle size, we obtained kinetic parameters following the procedure detailed in our previous study [14,22]. The size decrease rate is modeled using a modified Arrhenius expression,

$$\dot{D}_p = -A_{nm} T^{1/2} \exp\left[-\frac{E_a}{RT}\right], \quad (1)$$

where  $A_{nm}$  is an initial size-dependent preexponential factor and  $E_a$  is a size-independent activation

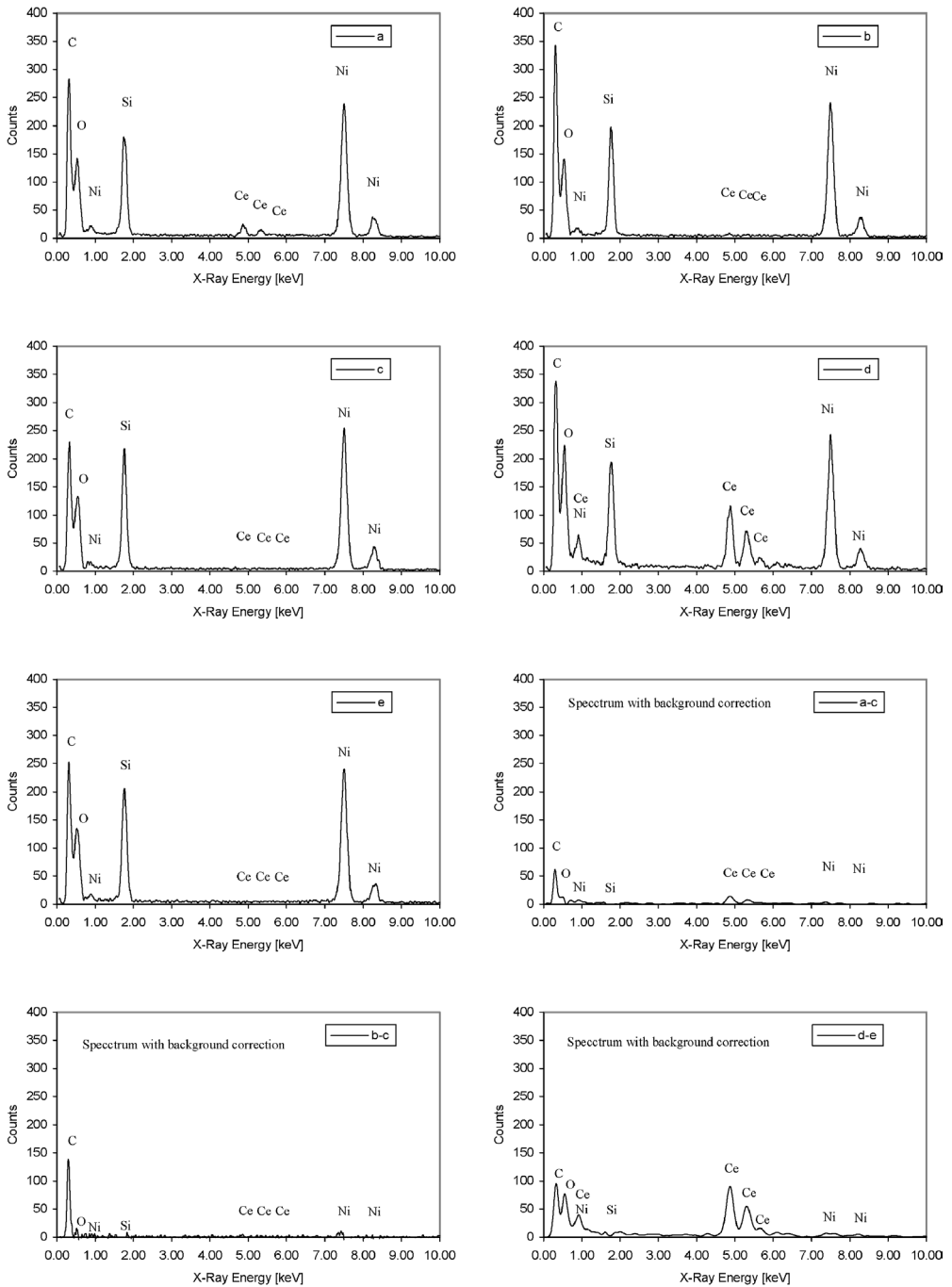


Fig. 9. EDS spectra of cerium-laden diesel particles with and without background noise correction. Legends correspond to spots marked in Fig. 8. Minus sign in the legend means background noise correction.

energy. Values of  $A_{nm}$  and  $E_a$  were determined by integrating

$$\Delta D_p = \int_0^X \frac{\dot{D}_p(x)}{u(x)} dx, \quad (2)$$

where  $x$  is the horizontal position in the tube,  $X$  is the length of the tube, and  $u$  is the flow velocity over the heated length of the flow tube. The differences between calculated and measured  $\Delta D_p$  values were minimized using a nonlinear least-squares method. The dependence of the size decrease rate and flow

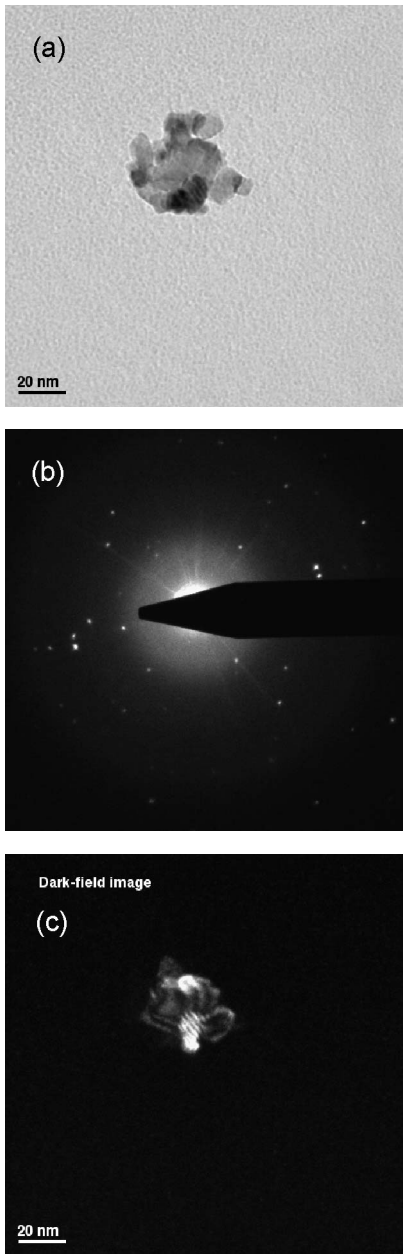


Fig. 10. (a) TEM image of a cerium aggregate. (b) Electron beam diffraction pattern. (c) Dark-field image.

velocity on horizontal position is a result of their dependence on temperature as seen in Eq. (1) and

$$u(x) = \frac{4}{3} u_m \frac{T(x)}{T_0}, \quad (3)$$

where  $u_m$  is the mean flow velocity calculated from the volume flow rate and the cross-sectional area of the flow tube, and  $\frac{4}{3}u_m$  is the peak volumetric flow velocity assuming laminar flow.

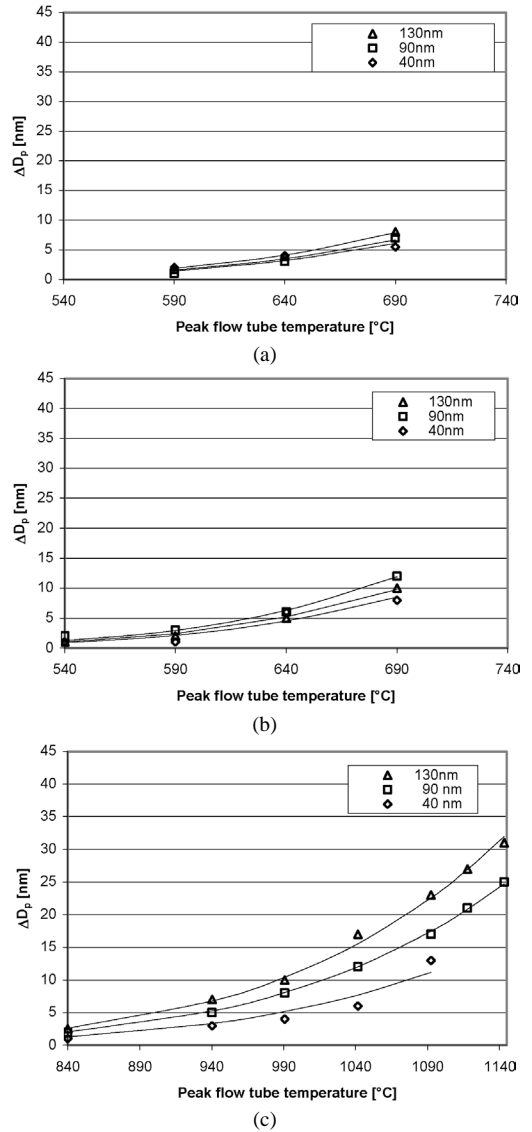


Fig. 11. Particle size change as a function of peak flow tube temperature for the three initial particle sizes: (a) 25 ppm cerium-dosed fuel, (b) 100 ppm cerium-dosed fuel, (c) regular base fuel [14].

Size decreases due to oxidation were determined relative to the size of the particles at 300 °C. This is lower than the temperature we used in our previous studies, 500 °C [14,22]. It was necessary to lower the base temperature because of the increased reactivity of the diesel particles on the addition of metal additives.

#### 4.4. Kinetic rates

Fig. 11 shows experimentally determined size reductions at various oxidation temperatures for 41-

92-, and 132-nm particles at 25 ppm (Fig. 11a) and 100 ppm (Fig. 11b) cerium doping levels. For comparison purposes, we also show in Fig. 11c results from our prior work on undosed diesel oxidation. One of the obvious differences seen between this work and the undosed results is the absence of any size-dependent oxidation. In the undosed case, we observed an increase in the apparent oxidation rate with increasing initial particle size. That result was investigated in our previous study [14] to correct the rates for the effective density of soot, which were measured [25] using an aerosol particle mass analyzer. Park et al. [25] observed that the effective density increases as particle size decreases and that normalization to the effective density results in an effective oxidation rate that was essentially particle size independent [14]. At this point, we do not have a definitive explanation of the differences observed between the dosed and undosed cases; however, it is possible that the nature of the soot structure in the dosed case is different and it is also possible that the mass fraction of cerium in the soot particles is size dependent. All that can be concluded without further investigation is that the apparent oxidation rate for dosed diesel is size invariant.

For practical convenience, we define the light-off temperature of oxidation as the peak flow tube temperature, where the particle shrinks  $\sim 1$  nm (in addition to the shrinkage arising from thermal evaporation). The light-off temperature was determined to be  $\sim 840$  °C for the undosed diesel particles as shown in Fig. 11c, but decreased significantly to 540 and 590 °C, respectively, for the 25 and 100 ppm dosing levels, as shown in Figs. 11a and 11b. The results suggest that the catalyst fulfilled a major, practical objective of decreasing the thermal budget of a DPF and that, after a threshold concentration, there is little benefit to operating at higher doping levels.

The data in Figs. 11a and 11b were fitted to an Arrhenius expression (Eq. (1)) and are shown as solid lines in the plot. Table 1 lists the Arrhenius parameters (frequency factors,  $A_{nm}$ , and activation energy,  $E_a$ ) obtained, and Fig. 12 shows an Arrhenius plot of the surface-specific oxidation rates for this study in comparison with selected prior studies. The activation energies of diesel particle oxidation for 25 and 100 ppm cerium dosing were essentially equivalent, within experimental error, and equaled 107 and

102  $\text{kJ mol}^{-1}$ , respectively. More interesting, perhaps, is that the activation energy of the dosed fuel was not any different from that of the undosed case (108  $\text{kJ mol}^{-1}$ ), even though the absolute oxidation rate in the range of temperature studies was some  $\sim 20$  times faster! These results are qualitatively consistent with the study by Stanmore et al. [26]. Using the thermogravimetric method, they compared oxidation rates of cerium-dosed diesel particles with that of undosed diesel particles under various engine conditions (idle, medium speed, high speed). They found that the presence of the catalyst did not change the activation energy, consistent with our observation; however, their measured activation energy (210  $\text{kJ mol}^{-1}$ ) was a factor of 2 higher than our observation. Miyamoto et al. [6] also found an increase in the oxidation rate (Fig. 12g) for Ca-catalyzed DPM. However, they observed a two-stage oxidation process. In their TGA study, they observed an initial stage of rapid oxidation with very low activation energy (Fig. 12h), followed by slower and higher activation energy kinetics (Fig. 12g) similar in magnitude to other studies. This rapid early stage is similar to an observation referred to as *auto-acceleration* by Lahaye et al. [9]. While our experiments are unable to resolve transients such as described above, we do note that the general addition of metals does not seem to change the activation energy, but does increase the oxidation rate significantly.

This corroborated observation that the use of a catalyst did not reduce the activation energy is, at this point, a mystery. We have previously observed that diesel soot oxidation has a lower activation energy than flame-generated soot; it has been speculated that small quantities of metals from lube oil may serve as an inadvertent catalyst [14,22]. This would at least provide a consistent picture for the observed results, although further work is still needed to establish if, indeed, sufficient metals from lube oil are incorporated into soot. Stanmore et al. [26] observed the fall-off in reactivity above 600 °C for cerium-dosed particles, which was not observed in our work. It is possible that the so-called auto-acceleration may be an artifact of the TGA measurements, which are notorious for being corrupted by mass and heat transfer effects as demonstrated by Mahadevan et al. [27]. From a practical point of view, the similarity of Ca and Ce suggests that other metals may serve as oxidant accelerators, leaving one to choose the dopant based on cost, ease of use, and environmental/health concerns, as well as oxidation rate.

Literature on the health effects of cerium additives is limited. A report [28] from the Health Effect Institute was the only extensive study we could find on the health effects of cerium additives. The report concluded that the risk of inhaling cerium at the estimated

Table 1

	25 ppm	100 ppm
$E_a$ ( $\text{kJ mol}^{-1}$ )	107	102
$A_{40}$ ( $10^5 \text{ nm K}^{-1/2} \text{ s}^{-1}$ )	6.6	5.0
$A_{90}$ ( $10^5 \text{ nm K}^{-1/2} \text{ s}^{-1}$ )	7.3	7.0
$A_{130}$ ( $10^5 \text{ nm K}^{-1/2} \text{ s}^{-1}$ )	8.6	5.8

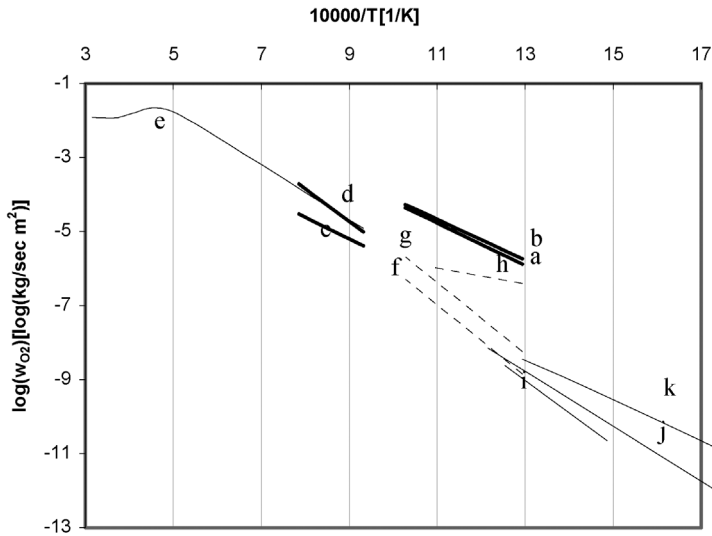


Fig. 12. Arrhenius plot of the surface-specific rates of diesel particle oxidation for the current study and for other relevant prior studies. Previous studies include oxidation rates of various soots (diffusion flame soot and carbon black) and pyrographite rod. (a) Current study (25 ppm cerium-dosed case). (b) Current study (100 ppm cerium-dosed case). (c) Diesel particles with regular fuel [14]. (d) Diffusion flame-generated soot [22]. (e) Nagle and Strickland-Constable [29] using a pyrographite rod. (f) TGA of uncatalyzed diesel soot [6]. (g) TGA of catalyzed (Ca added to fuel) diesel soot [6]. (h) TGA of catalyzed (Ca added to fuel) diesel soot, rapid stage oxidation [6]. (i) Flow reactor study of Printex-U flame soot from Degussa AG [30]. (j) TGA of diesel particle [31]. (k) Flow reactor study of diesel particles [32].

worst-case ambient level ( $1.2 \mu\text{g}/\text{m}^3$ ) arising from heavy diesel traffic, using a cerium additive with a particulate trap, appears to be small. However, the absence of more complete information precluded their fully assessment of the possible health effects of using cerium as a fuel additive. They mentioned that risk of chronic exposure was more difficult to estimate due to the lack of adequate studies and the possible increase in cerium emissions during regeneration of the particulate trap. It should be further noted that no one is proposing the use of Ce or any metal as a soot suppression additive on its own. It would only be used in combination with a particle filter. Used in this manner Ce has a double benefit: it reduces the amount of soot collected in the filter, and thus the frequency of regeneration, and facilitates regeneration when it occurs.

## 5. Conclusion

The influence of a cerium additive on the kinetics of ultrafine diesel particle oxidation has been measured using a HTO-TDMA method. The addition of cerium was observed to cause significant changes in number-weighted size distributions, light-off temperature, and the kinetics of oxidation.

- Cerium addition decreased the peak number concentrations in the accumulation modes by 50 and

65%, respectively, at the 25 and 100 ppm dosing levels (1400 rpm, 75% engine load). Nuclei mode particles, most likely occurring as cerium oxide, appeared as the cerium dosing rate increased.

- The light-off temperature was reduced by 250 and 300 °C, respectively, at 25 and 100 ppm cerium.
- The oxidation rate increased significantly ( $\times 20$ ) with addition of cerium to the fuel. However, the rate was relatively insensitive to doping level, suggesting that, beyond a certain threshold level, no further benefit can be obtained by higher doping. The activation energy for cerium-dosed oxidation was within experimental error and equivalent to that of undosed fuel ( $E_a = 100\text{--}110 \text{ kJ mol}^{-1}$ ). From a phenomenological kinetic rate perspective, the increase in oxidation rate is attributed solely to an increase in the pre-exponential factor. In a prior study, we found that the oxidation rates of diesel particles and flame soot [14,22] are very different. In particular, the activation energy for the oxidation of diesel particles was  $108 \text{ kJ mol}^{-1}$ , significantly lower than the value of  $164 \text{ kJ mol}^{-1}$  for flame soot; despite this, diesel soot actually oxidized more slowly than flame soot over the temperature range measured. These results suggest that diesel particles, using regular undosed diesel fuels, are already metal catalyzed to some extent, most likely from

metals in the lube oil. The addition of cerium likely increases the number of catalytic sites (observed as an increase in frequency factors) but has no effect on the overall activation energy due to the presence of other metals in the DPM coming from lube oil.

## Acknowledgments

Authors gratefully acknowledge Rhodia Electronics & Catalysis for supplying us with their cerium-based fuel additive. The authors also thank Dr. Art Miller (NIOSH) for his review and comments, and Dr. McKernan (University of Minnesota) for EDS analysis.

## References

- [1] J.J. Tutko, S.S. Lestz, J.W. Brockmeyer, J.E. Dore, SAE Technical Paper 840073 (1984).
- [2] K.J. Baumgard, D.B. Kittelson, SAE Technical Paper 850009 (1985).
- [3] G. Lepperhoff, G. Kroon, SAE Technical Paper 850013 (1985).
- [4] J. van Doorn, J. Varloud, P. Meriaudeau, V. Perrichon, M. Chevrier, C. Gauthier, Appl. Catal. B 1 (1992) 117–127.
- [5] N. Miyamoto, H. Zhixin, A. Harada, H. Ogawa, T. Murayama, SAE Technical Paper 871612 (1987).
- [6] N. Miyamoto, H. Zhixin, O. Hideyuki, SAE Technical Paper 881224 (1988).
- [7] J.M. Valentine, J.D. Peter-Hoblyn, G.K. Acres, SAE Technical Paper 2000-01-1934 (2000).
- [8] G. Skillas, Z. Qian, U. Baltensperger, U. Matter, H. Burtscher, Combust. Sci. 154 (2000) 259–273.
- [9] J. Lahaye, S. Boehm, P.H. Chambrion, P. Ehrburger, Combust. Flame 104 (1996) 199–207.
- [10] M. Kasper, K. Sattler, K. Siegmann, U. Matter, H.C. Siegmann, J. Aerosol Sci. 30 (1999) 217.
- [11] K. Pattas, N. Kyriakis, Z. Samaras, T. Manikas, A. Mihailidis, W. Mustel, P. Rouveiroles, SAE Technical Paper 980543 (1998).
- [12] N. Kyriakis, Z. Samaras, E. Vouitsis, T. Manikas, T. Seguelong, G. Blanchard, SAE Technical Paper 2002-01-0429 (2002).
- [13] S.C. Wang, R.C. Flagan, Aerosol Sci. Technol. 13 (1990) 230–240.
- [14] K.J. Higgins, H. Jung, D.B. Kittelson, J.T. Roberts, M.R. Zachariah, Environ. Sci. Technol. 37 (2003) 1949–1954.
- [15] I. Abdul-Khalek, D.B. Kittelson, F. Brear, The Influence of Dilution Conditions on Diesel Exhaust Particle Size Distribution Measurements, SAE Technical Paper 1999-01-1142 (1999).
- [16] H. Jung, D.B. Kittelson, M.R. Zachariah, Combust. Flame 136 (2003) 445–456.
- [17] S.N. Rogak, R.C. Flagan, H.V. Nguyen, Aerosol Sci. Technol. 18 (1993) 25.
- [18] D.B. Kittelson, J. Aerosol Sci. 29 (1998) 575–588.
- [19] I. Abdul-Khalek, D.B. Kittelson, Real Time Measurement of Volatile and Solid Exhaust Particles Using a Catalytic Stripper, SAE Technical Paper 950236 (1995).
- [20] I.P. Ng, Aethalometer Performance with Diesel Particles, in: Mechanical Engineering, University of Minnesota, Twin Cities, 2002.
- [21] H. Sakurai, H.J. Tobias, K. Park, D. Zurling, K.S. Docherty, D.B. Kittelson, P.H. McMurry, P.J. Ziemann, Atmos. Environ. 37 (2003) 1199–1210.
- [22] K.J. Higgins, H. Jung, D.B. Kittelson, J.T. Roberts, M.R. Zachariah, J. Phys. Chem. A 106 (2002) 96–103.
- [23] S.V. Hering, S.K. Friedlander, J.J. Collins, L.W. Richards, Environ. Sci. Technol. 13 (1979) 184–188.
- [24] A. Miller, G. Ahlstrand, D.B. Kittelson, M.R. Zachariah, The Fate of Metal (Fe) During Diesel Combustion: Nanoparticle Formation, Morphology and Chemistry, 2005, in preparation.
- [25] K. Park, C. Feng, D.B. Kittelson, P.H. McMurry, Environ. Sci. Technol. 37 (2003) 577–583.
- [26] B. Stanmore, B.J.-F., P. Gilot, The Ignition and Combustion of Cerium Doped Diesel Soot, SAE Technical Paper 1999-01-0115 (1999).
- [27] R. Mahadevan, D. Lee, H. Sakurai, M.R. Zachariah, J. Phys. Chem. A 106 (2002) 11,083–11,092.
- [28] M.G. Costantini, R. Henderson, D.S. Greenbaum, H. Greim, E.D. Pellizzari, R. Sawyer, J. Warren, J. Ball, S. Cadle, J.M. Davis, N. Englert, D.B. Kittelson, A. Mayer, J. McAughey, R. McClellan, R.F. Phalen, G. Simon, M. Waalkes, Health Effects Inst. Commun. 9 (2001).
- [29] J. Nagle, R.F. Strickland-Constable, in: Fifth Carbon Conference, Pergamon, Oxford, 1962.
- [30] J.P.A. Neeft, T.X. Nijhuis, E. Smakman, M. Makkee, J.A. Moulijn, Fuel 76 (1997) 1129.
- [31] K. Otto, M.H. Sieg, M. Zinbo, L. Bartosiewicz, SAE Technical Paper 800336 (1980).
- [32] A.F. Ahlström, C.U.I. Odenbrand, Carbon 3 (1989) 475.